EPJ Web of Conferences **175**, 05013 (2018) https://doi.org/10.1051/epjconf/201817505013
Lattice 2017

Baryon interactions from lattice QCD with physical masses —$S = -3$ sector: $\Xi\Sigma$ and $\Xi\Lambda$-$\Xi\Sigma$—

Noriyoshi Ishii[1,2,⋆], *Sinya* Aoki[3,4], *Takumi* Doi[2,5], *Shinya* Gongyo[2], *Tetsuo* Hatsuda[2,5], *Yoichi* Ikeda[1,2], *Takashi* Inoue[2,6], *Takumi* Iritani[2], *Takaya* Miyamoto[2,3], *Hidekatsu* Nemura[1,2], and *Kenji* Sasaki[2,3]

[1] *RCNP, Osaka university, 10-1 Mihoga-oka, Ibaraki-shi, Osaka, 567-0047, Japan*
[2] *Theoretical Research Division, Nishina Center, RIKEN, Wako 351-0198, Japan*
[3] *Center for Gravitational Physics, Yukawa Institute for Theoretical Physics, Kyoto University, Kyoto 606-8502, Japan*
[4] *Center for Computational Sciences, University of Tsukuba, Tsukuba 305-8577, Japan*
[5] *iTHEMS Program and iTHES Research Group, RIKEN, Wako 351-0198, Japan*
[6] *Nihon University, College of Bioresource Sciences, Kanagawa 252-0880, Japan*

Abstract. Hyperon-nucleon and hyperon-hyperon interactions are important in studying the properties of hypernuclei in hypernuclear physics. However, unlike the nucleons which are quite stable, hyperons are unstable so that the direct scattering experiments are difficult, which leads to the large uncertainty in the phenomenological determination of hyperon potentials. In this talk, we use the gauge configurations generated at the (almost) physical point ($m_\pi = 146$ MeV) on a huge spatial volume $(8.1\text{fm})^4$ to present our latest result on the hyperon-hyperon potentials in $S = -3$ sector ($\Xi\Sigma$ single channel and $\Xi\Sigma$-$\Xi\Lambda$ coupled channel) from the Nambu-Bethe-Salpeter wave functions based on the HAL QCD method with improved statistics.

1 Introduction

Experimental determination of hyperon-nucleon (YN) and hyperon-hyperon (YY) interactions is one of the most important subjects of J-PARC. These hyperon interactions are important in studying the structure of hyper nuclei. They are also important in studying the structure of the neutron stars through the equation of states at high density. However, hyperons are too unstable to be used in a direct scattering experiment so that the phenomenological determination of hyperon potentials involves large uncertainty. Since the uncertainty increases as the number of strange quarks increases, they mainly focus on $S = -1$ and $S = -2$ sectors in J-PARC. In contrast, lattice QCD (LQCD) determination of these potentials which was recently developed by HAL QCD Collaboration [1, 2, 3, 4, 5] becomes easier for the increasing number of strange quarks. In this talk, we present our results of hyperon-hyperon potentials for $S = -3$ sector ($\Xi\Sigma$(I=3/2) single channel and $\Xi\Lambda$-$\Xi\Sigma$(I=1/2) coupled channel) with improved statistics by using 2+1 flavor LQCD gauge configurations generated by employing almost the physical pion mass $m_\pi \simeq 146$ MeV by using K computer at AICS [6].

⋆Speaker, e-mail: ishiin@rcnp.osaka-u.ac.jp

2 Lattice QCD setup

We use the 2+1 flavor gauge configurations at almost the physical point generated on 96^4 lattice where the RG improved (Iwasaki) gauge action and the nonperturbatively $O(a)$-improved Wilson quark (clover) action are employed at $\beta = 1.82$, $(\kappa_{\rm ud}, \kappa_{\rm s}) = (0.126117, 0.12790)$ with $c_{\rm SW} = 1.11$ and the 6-APE stout smeared links with the smearing parameter $\rho = 0.1$ [6]. The setup leads to the lattice spacing $a^{-1} \simeq 2.3$ GeV ($a \simeq 0.085$ fm), the spatial extension $L = 96a \simeq 8.1$ fm, $m_\pi \simeq 146$ MeV and $m_K \simeq 525$ MeV. 400 gauge configurations are used for the measurement of hyperon potentials with the time-dependent HAL QCD method [5], where each gauge configuration is separated by 5 HMC trajectories. Quark propagators are generated with a wall source accepting the Coulomb gauge fixing, where we impose the periodic boundary condition on the spatial directions, whereas Dirichlet boundary condition is imposed on the temporal direction on the time slice $t = t_1$ which is separated from the wall source as $t_1 - t_0 = 48$. We use 48 source points for the measurement of the hyperon potentials. The charge conjugation and time reversal symmetries are used to combine the forward and backward propagation to double the statistics of two-point and four-point hyperon correlators, while the hypercubic symmetry of 96^4 lattice is used to quadruple the statistics. Statistical data are averaged in the bin of the size 20, which is equivalent to 100 HMC trajectories. Jackknife prescription is used to estimate the statistical errors.

3 Single baryon sector

We show the effective mass plots of the temporal two-point correlators of Λ, Σ and Ξ in Fig. 1 both for the point-sink and wall-source (point-wall) and for the wall-sink and wall-source (wall-wall). To obtain the mass m and the overlap parameters $a_{\rm PW}$ and $a_{\rm WW}$ for the point-wall and wall-wall correlators, we perform single exponential fit analysis of the point-wall and the wall-wall temporal two-point correlators by employing the functional form

$$C_{\rm PW}(t) \simeq a_{\rm PW} \exp(-mt), \qquad C_{\rm WW}(t) \simeq a_{\rm WW} \exp(-mt). \tag{1}$$

The overlap parameters are used to obtain the $\Xi\Lambda$-$\Xi\Sigma$(I=1/2) coupled channel potentials. They con-

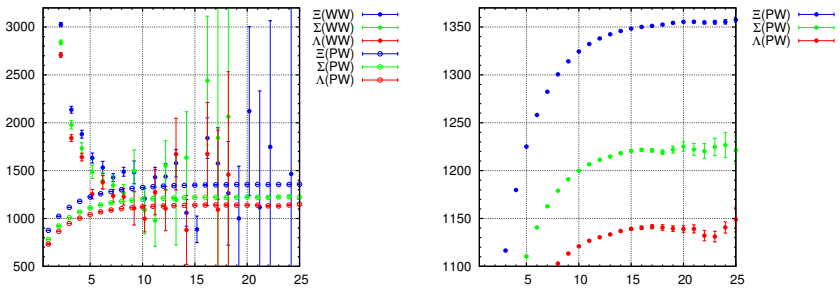

Figure 1. The effective mass plots of Λ, Σ and Ξ for (WW) wall-wall and (PW) point-wall (lhs) and those for point-wall correlators (rhs) for comparison.

tribute to the $\Xi\Lambda$-$\Xi\Sigma$ coupled channel potential in the combination $\sqrt{Z_\Lambda/Z_\Sigma}$. Here, Z_Λ and Z_Σ denote the Z factors of local composite hyperon operators for Λ and Σ hyperons, respectively, which appear in the limit $\psi(x) \to Z^{1/2}\psi_{\rm out}(x)$ as $x_0 \to +\infty$ where $\psi(x)$ and $\psi_{\rm out}(x)$ denote local composite hyperon

operators and the corresponding asymptotic fields. For point-wall correlators, we identify the plateau regions as 15-20 for Λ and Σ while 20-25 for Ξ. In contrast, the wall-wall correlators are too noisy to identify the plateau regions so that we examine the two regions (i) 10-15 and (ii) 15-20. The fit with 10-15 leads to $\sqrt{Z_\Lambda/Z_\Sigma} = 1.01(3)$, whereas the fit with 15-20 leads to $\sqrt{Z_\Lambda/Z_\Sigma} = 1.02(6)$. Since the results do not lead to a significant change, we adopt the result for 10-15. The results for the hyperon masses are given as follows: $m_\Lambda = 1.139(2)$ GeV, $m_\Sigma = 1.222(2)$ GeV and $m_\Xi = 1.356(2)$ GeV.

4 $\Xi\Sigma$ (I=3/2) single channel potentials

In order to obtain the $\Xi\Sigma$(I=3/2) single channel potential, we use the time-dependent HAL QCD method which allows us to extract the potential without requiring the ground state saturation [5]. We define the R-correlator for $\Xi\Sigma$ as

$$R(\vec{x}-\vec{y},t;\mathcal{J}_{\Xi\Sigma}) \equiv \left\langle 0 \left| T\left[\Xi(\vec{x},t)\Sigma(\vec{y},t)\cdot\mathcal{J}_{\Xi\Sigma}(t=0)\right]\right| 0\right\rangle / e^{-(m_\Xi+m_\Sigma)t}, \tag{2}$$

where $\Xi(x)$ and $\Sigma(y)$ denote local composite fields for Ξ and Σ, and $\mathcal{J}_{\Xi\Sigma}$ denotes the wall source for $\Xi\Sigma$. The R-correlator Eq. (2) satisfies the time-dependent Schrödinger-like equation for unequal mass system which involves a fourth time-derivative [7]. The $\Xi\Sigma$(I=3/2) single channel potential should be obtained from this equation. However, since the numerical evaluation of fourth time-derivative is unstable so far, we use its non-relativistic approximation. By keeping only the leading order of derivative expansion of the non-local potential, the time-dependent Schrödinger-like equation is given as

$$\left(-\frac{\partial}{\partial t}+\frac{\nabla^2}{2\mu}\right)R_{\Xi\Sigma}(\vec{r},t) = V_{\Xi\Sigma}(\vec{r})R_{\Xi\Sigma}(\vec{r},t), \tag{3}$$

where $\mu \equiv 1/(1/m_\Xi + 1/m_\Sigma)$ denotes the reduced mass.

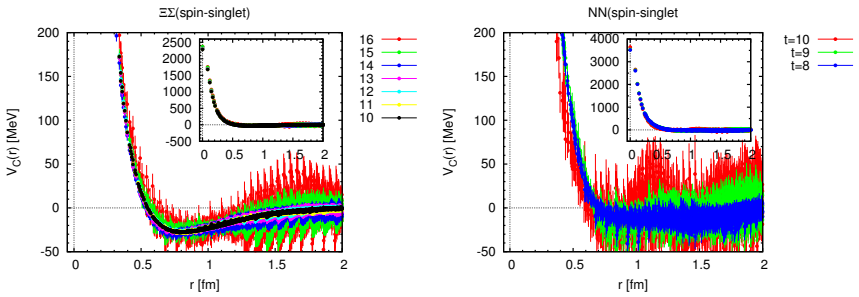

Figure 2. The spin-singlet central potential for $\Xi\Sigma$(I=3/2) single channel obtained from the t region $t = 10-16$ (lhs) together with the spin-singlet central potential for NN (I=1) from $t = 8-10$ (rhs) for comparison.

We show the spin-singlet central potential for $\Xi\Sigma$(I=3/2) single channel in Fig. 2(lhs), where the potentials obtained in the t region $t = 10-16$ are plotted. Since t-dependence is seen to be weak, we regard these potentials to converge. We see that the there is a repulsive core which is surrounded by an attractive pocket. In this way, the qualitative behavior is quite similar to the central NN potential. This is natural because, in the flavor SU(3) limit, $\Xi\Sigma$(I=3/2) belongs to flavor irrep. **27** to which NN(I=1) also belongs (dineutron channel). To see the size of the flavor SU(3) breaking, we show the spin-singlet NN potential for I=1 sector in Fig. 2 for comparison. (For detail of NN results, see

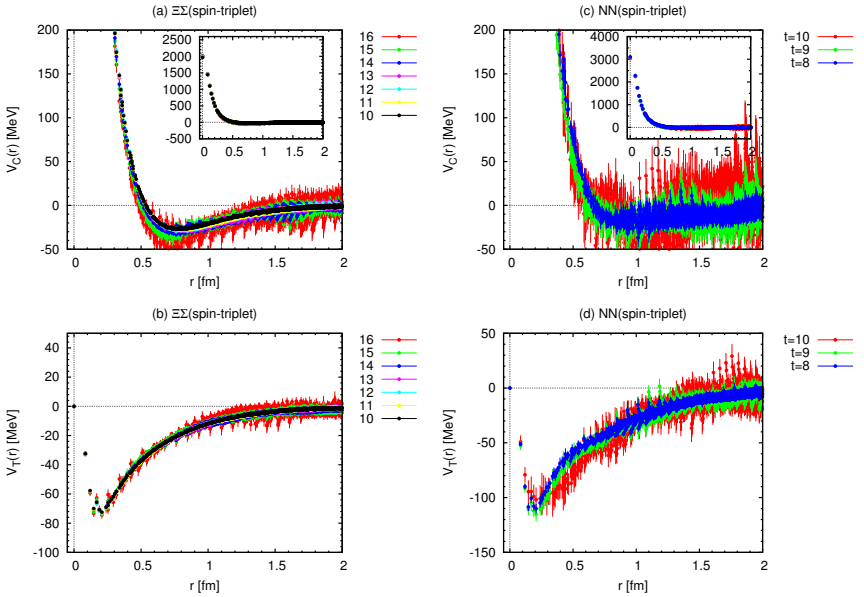

Figure 3. The spin-triplet ΞΣ(I=3/2) potential together with the spin-triplet NN potentials (I=0) for comparison. (a) ΞΣ central potential, (b) ΞΣ tensor potential, (c) NN central potential and (d) NN tensor potential.

Ref.[8].) We see that ΞΣ potential has a weaker repulsive core. However, the statistical noise of NN potential is too large to compare the attraction for middle to long distance.

The spin-triplet central and tensor potentials for ΞΣ(I=3/2) single channel are shown in Fig. 3(a) and (b). These potentials are obtained in the t region $t = 10 - 16$. Since the t dependence is seen to be weak again, we regard them to converge. We see that qualitative behaviors of these ΞΣ potentials are similar to those of NN. (We also show the spin-triplet central and tensor potentials for NN (I=0) in Fig. 3(c) and (d) for comparison.) This is natural because, in the flavor SU(3) limit, ΞΣ(I=3/2) belongs to flavor irrep. $\mathbf{10}^*$ to which NN(I=0) also belongs (deuteron channel). However, quantitatively, we see that there are some flavor SU(3) breaking effects, i.e., ΞΣ has a weaker repulsive core in the central potential and a weaker tensor force.

We use these ΞΣ(I=3/2) single channel potentials to solve Schrödinger equation for the scattering phase shift. Fig. 4(a) shows the scattering phase shift of ΞΣ(I=3/2) for ${}^1S_0$ channel. We see that the interaction is attractive but that it is not strong enough to generate a bound state. Thus the qualitative behavior is quite similar to NN case. Fig. 4(b),(c) and (d) show the scattering phase shifts and the mixing parameter of ΞΣ(I=3/2) for ${}^3S_1 - {}^3D_1$ channel. We see that the interaction is attractive but the strength is not strong enough to generate a bound state. Therefore, the qualitative behaviors are similar to NN except for the existence of the bound state (deuteron).

We make a comment on the t region used to calculate these potentials. In obtaining these ΞΣ potentials, we replace the exponential factor $e^{-(m_\Xi+m_\Sigma)t}$ of the R-correlator Eq. (2) by a product of temporal two point correlators (point-wall) of Ξ and Σ. We do this to expect a cancellation of the correlated statistical noises. Therefore, although the t dependence of these potentials are small, t should be large enough to achieve the ground state saturations of the temporal two-point correlators of Ξ and Σ, i.e, $t \lesssim 20$.

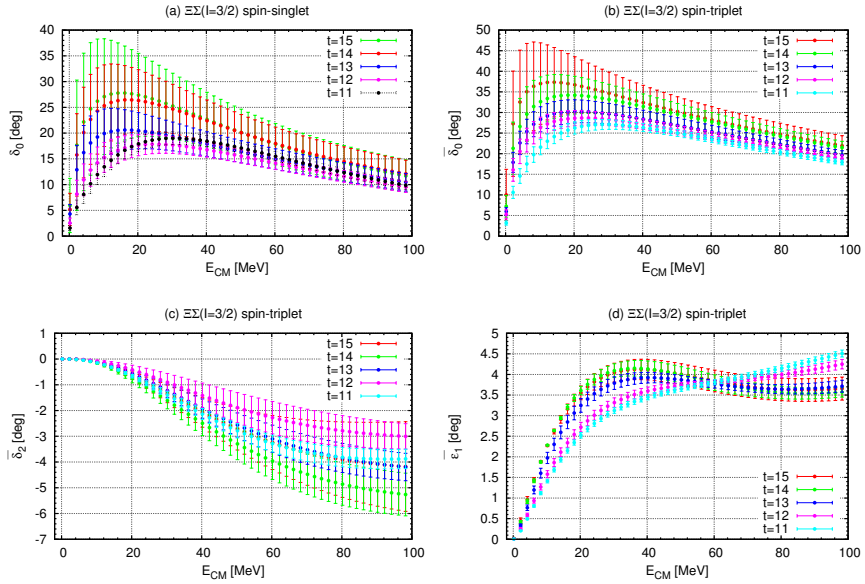

Figure 4. ΞΣ(I=3/2) scattering phase shifts from $t = 11-15$. (a) The s-wave phase shift $\delta_0(E)$ for ${}^1S_0$ channel, (b) s-wave phase shift $\bar{\delta}_0(E)$ for ${}^3S_1$-${}^3D_1$ channel, (c) d-wave phase shift $\bar{\delta}_2(E)$ for ${}^3S_1$-${}^3D_1$ channel and (d) mixing parameter $\bar{\epsilon}_1(E)$ for ${}^3S_1 - {}^3D_1$ channel.

5 ΞΛ-ΞΣ(I=1/2) coupled channel sector

We use a coupled channel extension of the time-dependent Schrödinger-like equation to obtain the ΞΛ-ΞΣ(I=1/2) coupled channel potentials. To use this equation, we define the R-correlators as

$$R_{\Xi\Lambda}(\vec{x}-\vec{y},t;\mathcal{J}) \equiv \left\langle 0\left|T\left[\Xi(\vec{x},t)\Lambda(\vec{y},t)\cdot\mathcal{J}(t=0)\right]\right|0\right\rangle / e^{-(m_\Xi+m_\Lambda)t} \quad (4)$$

$$R_{\Xi\Sigma}(\vec{x}-\vec{y},t;\mathcal{J}) \equiv \left\langle 0\left|T\left[\Xi(\vec{x},t)\Sigma(\vec{y},t)\cdot\mathcal{J}(t=0)\right]\right|0\right\rangle / e^{-(m_\Xi+m_\Sigma)t}, \quad (5)$$

where $\Xi(x)$, $\Lambda(y)$ and $\Sigma(y)$ denote local composite operators for Ξ, Λ and Σ, respectively. $\mathcal{J} = \mathcal{J}_{\Xi\Lambda}$ and $\mathcal{J}_{\Xi\Sigma}$ denotes the wall source for ΞΛ and ΞΣ, respectively. The coupled channel extension of the time-dependent Schrödinger-like equation for unequal mass system involves fourth time-derivative [7]. However, since the numerical evaluation of fourth time-derivative is still unstable, we use its non-relativistic approximation as

$$\begin{bmatrix} \left(-\frac{\partial}{\partial t}+\frac{\nabla^2}{2\mu_{\Xi\Lambda}}\right)R_{\Xi\Lambda}(\vec{r},t;\mathcal{J}) \\ \left(-\frac{\partial}{\partial t}+\frac{\nabla^2}{2\mu_{\Xi\Sigma}}\right)R_{\Xi\Sigma}(\vec{r},t;\mathcal{J}) \end{bmatrix} = \begin{bmatrix} V_{\Xi\Lambda;\Xi\Lambda}(\vec{r}) & \zeta_0\zeta^{+t/a}V_{\Xi\Lambda;\Xi\Sigma}(\vec{r}) \\ \zeta_0^{-1}\zeta^{-t/a}V_{\Xi\Sigma;\Xi\Lambda}(\vec{r}) & V_{\Xi\Sigma;\Xi\Sigma}(\vec{r}) \end{bmatrix} \cdot \begin{bmatrix} R_{\Xi\Lambda}(\vec{r},t;\mathcal{J}) \\ R_{\Xi\Sigma}(\vec{r},t;\mathcal{J}) \end{bmatrix}, \quad (6)$$

where $\zeta \equiv e^{(m_\Sigma-m_\Lambda)a}$ and $\zeta_0 \equiv \sqrt{Z_\Lambda/Z_\Sigma}$. $\mu_{\Xi\Lambda} \equiv 1/(1/m_\Xi + 1/m_\Lambda)$ and $\mu_{\Xi\Sigma} \equiv 1/(1/m_\Xi + 1/m_\Sigma)$ denote the reduced mass for ΞΛ and ΞΣ, respectively. We use Eq. (6) twice by replacing the source by $\mathcal{J} = \mathcal{J}_{\Xi\Lambda}$ and $\mathcal{J}_{\Xi\Sigma}$ to obtain these four coupled channel potentials.

Fig. 5 shows the spin-singlet ΞΛ-ΞΣ (I=1/2) coupled channel central potentials obtained from t region $t = 10-16$. We see that they are quite noisy. t-dependence is mild except for the the long

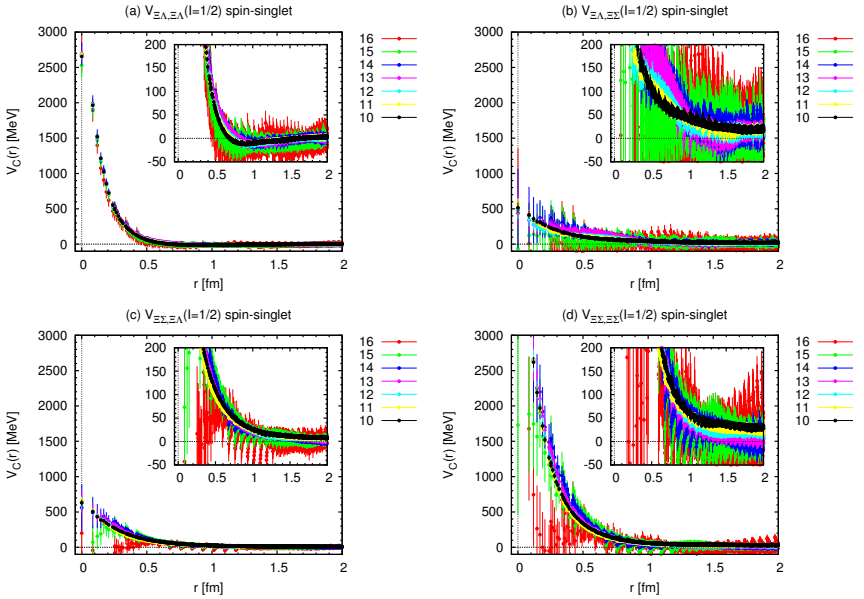

Figure 5. The spin-singlet central potentials for ΞΛ-ΞΣ(I=1/2) coupled channel from $t = 10-16$. (a) $V_{C;\Xi\Lambda,\Xi\Lambda}(r)$, (b) $V_{C;\Xi\Lambda,\Xi\Sigma}(r)$, (c) $V_{C;\Xi\Sigma,\Xi\Lambda}(r)$ and (d) $V_{C;\Xi\Sigma,\Xi\Sigma}(r)$.

distance behavior of $V_{C;\Xi\Lambda,\Xi\Sigma}(r)$ and $V_{C;\Xi\Sigma,\Xi\Sigma}(r)$. Note that qualitative behaviors of these potentials can be understood in terms of the flavor SU(3) symmetry, i.e., in the flavor SU(3) limit, these potentials are expressed as linear combinations of two potentials $V_{\mathbf{27}}(r)$ and $V_{\mathbf{8_S}}(r)$ for the irreps. **27** and $\mathbf{8_S}$ of flavor SU(3) as $V_{\Xi\Lambda,\Xi\Lambda}(r) = \frac{9}{10}V_{\mathbf{27}}(r) + \frac{1}{10}V_{\mathbf{8_S}}(r)$, $V_{\Xi\Lambda,\Xi\Sigma}(r) = -\frac{3}{10}V_{\mathbf{27}}(r) + \frac{3}{10}V_{\mathbf{8_S}}(r)$, $V_{\Xi\Sigma,\Xi\Lambda}(r) = -\frac{3}{10}V_{\mathbf{27}}(r)+\frac{3}{10}V_{\mathbf{8_S}}(r)$ and $V_{\Xi\Sigma,\Xi\Sigma}(r) = \frac{1}{10}V_{\mathbf{27}}(r)+\frac{9}{10}V_{\mathbf{8_S}}(r)$, which explains, in particular, (i) the existence of an attractive pocket in $V_{C;\Xi\Lambda,\Xi\Lambda}(r)$ and (ii) very strong repulsive core of $V_{C;\Xi\Sigma,\Xi\Sigma}(r)$. (For lattice QCD results of $V_{C;\mathbf{27}}(r)$ and $V_{C;\mathbf{8_S}}(r)$ in the flavor SU(3) limit, see Ref.[9].)

Fig. 6 and Fig. 7 show the spin triplet ΞΛ-ΞΣ (I=1/2) coupled channel central and tensor potentials obtained from t region $t = 10-16$. t dependence is seen to be mild. Their qualitative behaviors can be understood by the flavor SU(3) symmetry again. As before, in the flavor SU(3) limit, these potentials are expressed as linear combinations of the two potentials $V_{\mathbf{10}}(r)$ and $V_{\mathbf{8_A}}(r)$ for the flavor SU(3) irreps. **10** and $\mathbf{8_A}$ as $V_{\Xi\Lambda,\Xi\Lambda}(r) = V_{\Xi\Sigma,\Xi\Sigma}(r) = \frac{1}{2}V_{\mathbf{10}}(r)+\frac{1}{2}V_{\mathbf{8_A}}(r)$ and $V_{\Xi\Lambda,\Xi\Sigma}(r) = V_{\Xi\Sigma,\Xi\Lambda}(r) = \frac{1}{2}V_{\mathbf{10}}(r)-\frac{1}{2}V_{\mathbf{8_A}}(r)$, which explains, in particular, (i) existence of an attractive pocket for $V_{C;\Xi\Lambda,\Xi\Lambda}(r)$ and $V_{C;\Xi\Sigma,\Xi\Sigma}(r)$, (ii) weak tensor potentials of ΞΛ-ΞΣ and ΞΣ-ΞΛ.

6 Summary

We have presented our "physical point" lattice QCD results of hyperon-hyperon potentials in $S = -3$ sector, i.e., ΞΣ(I=3/2) single channel potentials and ΞΛ-ΞΣ(I=1/2) coupled channel potentials, with improved statistics. We have used the 2+1 flavor QCD gauge configuration at almost the physical point ($m_\pi \simeq 146$ MeV) on the huge spatial volume $L \simeq 8.1$ fm generated on 96^4 lattice by K computer at AICS. To obtain these potentials, we have used a non-relativistic approximation of the time-

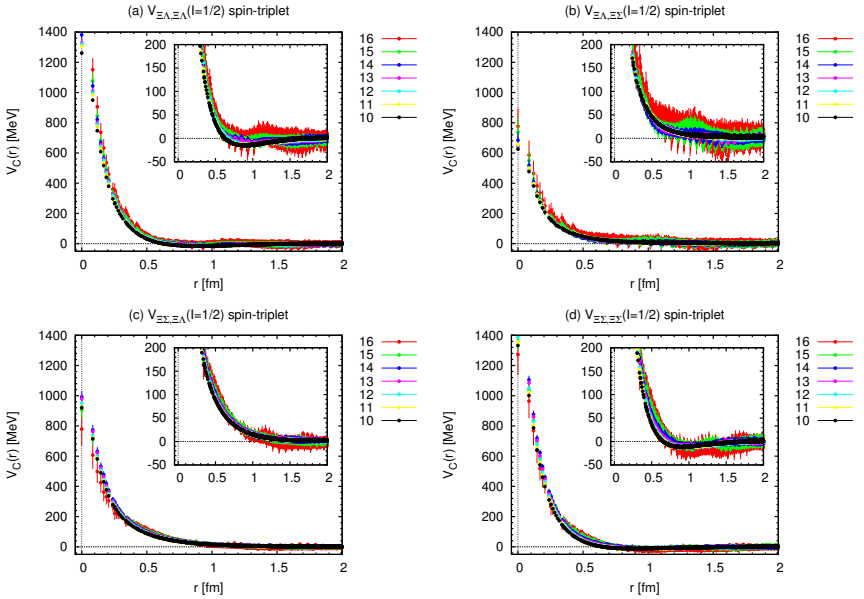

Figure 6. The spin-triplet central potentials for ΞΛ-ΞΣ(I=1/2) coupled channel from $t = 10 - 16$. (a) $V_{C;\Xi\Lambda,\Xi\Lambda}(r)$, (b) $V_{C;\Xi\Lambda,\Xi\Sigma}(r)$, (c) $V_{C;\Xi\Sigma,\Xi\Lambda}(r)$ and (d) $V_{C;\Xi\Sigma,\Xi\Sigma}(r)$.

dependent Schrödinger-like equation. We have seen that qualitative behaviors are similar to those expected from the flavor SU(3) symmetry, where mild SU(3) breaking effects are involved.

Acknowledgments

We thank members of PACS Collaboration for the gauge configuration generation. Lattice QCD calculations have been performed on K computer at RIKEN, AICS (Nos. hp120281, hp130023, hp140209, hp150223, hp150262, hp160211, hp170230), HOKUSAI FX100 computer at RIKEN, Wako (G15023, G16030, G17002) and HA-PACS at University of Tsukuba (Nos. 14a-20, 15a-30). We thank ILDG/JLDG [10] which serves as an essential infrastructure in this study. This work is supported in part by MEXT Grand-in-Aid for Scientific Research JP25400244, SPIRE (Strategic Program for Innovative REsearch) Field 5 project and "Priority Issue on Post-K computer" (Elucidation of the Fundamental Laws and Evolution of the Universe) and Joint Institute for Computational Fundamental Science (JICFuS).

References

[1] N. Ishii, S. Aoki and T. Hatsuda, Phys. Rev. Lett. **99** (2007) 022001 doi:10.1103/PhysRevLett.99.022001 [nucl-th/0611096].
[2] S. Aoki, T. Hatsuda and N. Ishii, Prog. Theor. Phys. **123** (2010) 89 doi:10.1143/PTP.123.89 [arXiv:0909.5585 [hep-lat]].
[3] S. Aoki *et al.* [HAL QCD Collaboration], Proc. Japan Acad. B **87** (2011) 509 doi:10.2183/pjab.87.509 [arXiv:1106.2281 [hep-lat]].

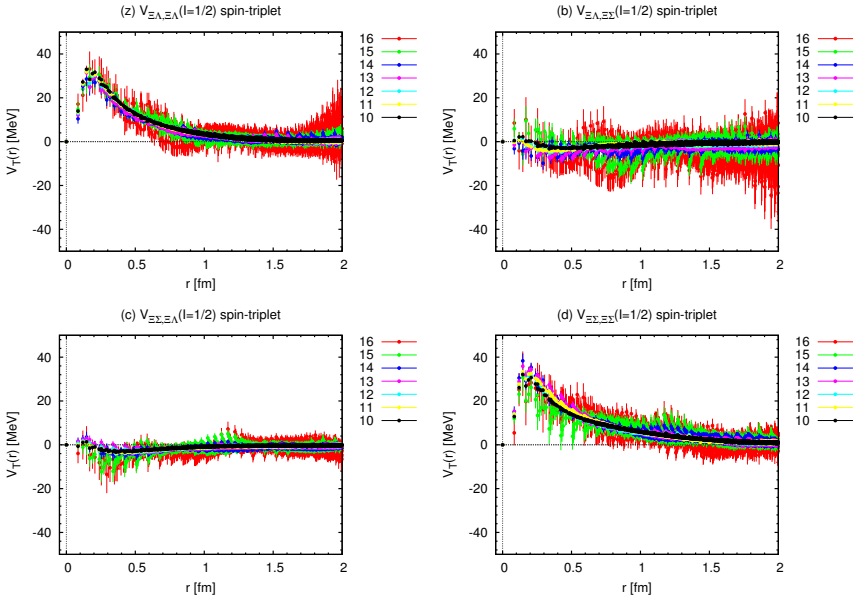

Figure 7. The tensor potentials for ΞΛ-ΞΣ(I=1/2) coupled channel from $t = 10 - 16$. (a) $V_{\mathrm{T};\Xi\Lambda,\Xi\Lambda}(r)$, (b) $V_{\mathrm{T};\Xi\Lambda,\Xi\Sigma}(r)$, (c) $V_{\mathrm{T};\Xi\Sigma,\Xi\Lambda}(r)$ and (d) $V_{\mathrm{T};\Xi\Sigma,\Xi\Sigma}(r)$.

[4] S. Aoki *et al.* [HAL QCD Collaboration], PTEP **2012** (2012) 01A105 doi:10.1093/ptep/pts010 [arXiv:1206.5088 [hep-lat]].
[5] N. Ishii *et al.* [HAL QCD Collaboration], Phys. Lett. B **712** (2012) 437 doi:10.1016/j.physletb.2012.04.076 [arXiv:1203.3642 [hep-lat]].
[6] K.-I. Ishikawa *et al.* [PACS Collaboration], PoS LATTICE **2015** (2016) 075 [arXiv:1511.09222 [hep-lat]].
[7] N. Ishii *et al.*, PoS LATTICE **2015** (2016) 087.
[8] T. Doi *et al.* [HAL QCD Collaboration], in these proceedings, arXiv:1711.01952[hep-lat].
[9] T. Inoue *et al.* [HAL QCD Collaboration], Nucl. Phys. A **881** (2012) 28 doi:10.1016/j.nuclphysa.2012.02.008 [arXiv:1112.5926 [hep-lat]].
[10] http://www.lqcd.org/ildg/ and http://www.jldg.org/